

# Classification of distinct tendinopathy subtypes for precision therapeutics

Received: 1 February 2024

Accepted: 22 October 2024

Published online: 01 November 2024



Chenqi Tang<sup>1,2,3,4,5,6,7,14</sup>, Zetao Wang<sup>1,2,3,4,6,7,8,14</sup>, Yuanhao Xie<sup>1,2,3,4,6,7,14</sup>, Yang Fei<sup>1,2,3,4,6,7</sup>, Junchao Luo<sup>1,2,3,4,6,7</sup>, Canlong Wang<sup>1,2,3,4,7</sup>, Yue Ying<sup>1,2,3,4,7</sup>, Peiwen He<sup>1,2,3,4,7</sup>, Ruojing Yan<sup>6</sup>, Yangwu Chen<sup>1,2,3,4,6,7</sup>, Jiayun Huang<sup>1,2,3,4,6,7</sup>, Yiwen Xu<sup>1,2,3,4,7</sup>, Zicheng Wang<sup>8</sup>, Boon Chin Heng<sup>10</sup>, Hengzhi Liu<sup>1,2,3,4,7</sup>, Jianyou Li<sup>8</sup>, Zi Yin<sup>2,6,7,11</sup>, Haobo Wu<sup>1,2,3,4</sup>, Weishan Chen<sup>1,2,3,4</sup>, Hongwei Ouyang<sup>1,2,3,4,5,6,7,11,12</sup>, Xiao Chen<sup>2,6,7,11</sup> & Weiliang Shen<sup>1,2,3,4,5,6,7,8,11,13</sup>✉

Rotator cuff tendinopathy is the most common tendinopathy type with the worst prognosis. Conventional treatments often elicit heterogeneous drug responses due to the diversity of tendinopathy. Hence, this study attempted a classification of 126 diseased tendons into three distinct subtypes with opposite pathogenic mechanisms based on transcriptomic and clinical features. The hypoxic atrophic subtype with white appearance (Hw) exhibits downregulated neovascularization pathways. The inflammatory proliferative subtype with white appearance (Iw) shows a moderate upregulation of inflammatory characteristics. The inflammatory proliferative subtype with red appearance (Ir) exhibits the highest levels of upregulated neovascularization and inflammatory pathways, along with severe joint dysfunction. We then established research models, including subtype-specific simulations in animal models and clinical data analysis. These revealed that glucocorticoid, a controversial commonly used drug, was only effective in treating the Ir subtype. Hence, the tendinopathy subtypes elucidated in this study have significant implications for developing precision treatment of tendinopathy.

Tendinopathy is a term used to describe a complex, multi-faceted tendon pathology characterized by pain and a dysfunctional joint condition, resulting in long-term or permanent deficits in tendon function. Up to 30% of general musculoskeletal consultations in primary care involve tendinopathy cases<sup>1</sup>. Rotator cuff tendinopathy is the most common type of tendinopathy, and is a major cause of shoulder pain, with up to half of the general population experiencing shoulder pain on at least one occasion per year<sup>2</sup>. The pathology of tendinopathy is complex and diverse, which is manifested as disordered fiber arrangement and destruction of fiber structures, along with increased cellularity in some parts and decreased cellularity in other parts of the diseased tissue. Other pathological changes such as cartilaginous metaplasia, ossification, increased blood vessels, and fat infiltration are also observed<sup>1</sup>.

Clinical treatment modalities for tendinopathy often elicit heterogeneous responses. The specific choice of treatment modality depends on the severity of tendinopathy, which is categorized into surgical or conservative treatment. Surgery is considered for severe tendinopathy. However, surgery has often yielded less than satisfactory results with considerable heterogeneity, and failure rates range from 11% to 94%<sup>3</sup>. Various intrinsic factors, such as age, tear size, muscle atrophy, fat infiltration, and retraction of tendons could diminish the beneficial effects of surgery<sup>3</sup>.

Conservative treatment modalities also often elicit heterogeneous drug responses. These methods can be employed to alleviate symptoms in patients with mild conditions. For instance, glucocorticoids have been widely used in tendon-related diseases, but their use

A full list of affiliations appears at the end of the paper. ✉ e-mail: [hwoy@zju.edu.cn](mailto:hwoy@zju.edu.cn); [chenxiao-610@zju.edu.cn](mailto:chenxiao-610@zju.edu.cn); [wshen@zju.edu.cn](mailto:wshen@zju.edu.cn)

remains a controversial issue<sup>1</sup>. Glucocorticoid therapy may not improve the prognosis<sup>4,5</sup> and, in some cases, may even prove to be detrimental<sup>6</sup>. However, some studies have suggested that glucocorticoid injections can alleviate pain and improve joint function<sup>7,8</sup> without increasing the risk of tendon re-tearing<sup>9</sup>. Currently, the classification of tendinopathy is primarily based on factors such as onset time, clinical symptoms, and the size and morphology of tear ruptures<sup>10,11</sup>. These classification methods are not a reliable guide for the selection of clinical drugs. Commonly utilized one size fits all treatment strategies have resulted in variable therapeutic efficacy among different tendinopathy subtypes. Accurately diagnosing and selecting appropriate patients for targeted treatment is expected to improve the current state of tendinopathy therapy.

In heterogeneous diseases such as colorectal cancer<sup>12</sup> and bladder cancer<sup>13</sup>, transcriptome sequencing can offer a deep insight into the pathology of the affected tissues, identifying their respective subtypes<sup>14–16</sup>. This can guide the practice of precision medicine, enhancing the therapeutic effectiveness of drugs. Therefore, we proposed a hypothesis that there may be different subtypes of tendinopathy.

In this work, we combine transcriptomic features with clinical characteristics to investigate the heterogeneity of tendinopathy and elucidate the underlying pathological mechanisms of different subtypes. We intend to identify animal models that can represent specific subtypes and validate differences in treatment efficacy. Furthermore, animal studies and clinical data analysis can help to identify treatment modalities that are more suitable for specific tendinopathy subtypes.

## Results

### Identification of three distinct subtypes of tendinopathy based on transcriptome profiles and clinical features

To better understand the heterogeneity of tendinopathy and identify potential subtypes, we collected clinical and transcriptomic data from 126 human-diseased tendons. The tear length of the diseased supraspinatus tendon was  $1.39 \pm 0.94$  cm in the coronal position and the tear width was  $1.27 \pm 0.58$  cm in the sagittal position. RNA-Seq analysis was performed on 126 diseased and 28 normal tendons. Principal component analysis (PCA) and heatmap of differentially expressed genes (DEGs) demonstrated a clear distinction between the transcriptomes of diseased and normal tendon samples (Supplementary Fig. 1A, B).

To identify distinct subgroups of tendinopathy patients, non-negative matrix factorization (NMF) consensus-clustering analysis was performed on our transcriptome profiles (Fig. 1A and Supplementary Fig. 1C). In the consensus clustering heatmap, the red color indicated a perfect agreement of the solution, while grayish white indicated no agreement. To determine the optimal number of clusters and assess the robustness of the clustering results, we computed cophenetic coefficients and average silhouette width for different cluster numbers from 2 to 7. Our analysis revealed that those patients were most appropriately divided into two subtypes. We also explored this analysis using the Brunet algorithm and obtained similar results. Therefore, based on the RNA-seq data, tendinopathy can be classified into two distinct molecular subtypes.

We then aimed to determine whether subgroups of tendinopathy exhibited molecular differences. The segregation of molecular subtypes was also reproducible by PCA (Fig. 1B). Among the different subtypes, one demonstrated a prominent upregulation in Hallmark pathways related to hypoxia, and we named this subtype Subtype H (Fig. 1C). In contrast, another subtype exhibited a significant upregulation in multiple inflammation associated pathways, and we named it Subtype I (Fig. 1C). Subtype H had the lowest xCell-inferred enrichment scores for multiple endothelial cells (Supplementary Fig. 2A). Conversely, Subtype I had the highest scores for various dendritic cell types (Supplementary Fig. 2B). These data thus highlighted that the two subtypes exhibited opposite pathological features, with Subtype H

showing elevated gene expression related to hypoxia, while Subtype I showed elevated gene expression associated with inflammation.

Next, we analyzed the differences in clinical features between the two subtypes. We ranked these features by p-value and selected the 10 features with the smallest p-values for presentation in Fig. 1D. We conducted binary logistic regression analysis on these 10 clinical features and calculated their odds ratio (OR). Among them, the color of the tendon had the highest OR, reaching 49.85 (Fig. 1D). Specifically, 94.7% of red hyperemia tendons were identified as Subtype I, while 73.5% of white non-hyperemia tendons were Subtype H. Based on this data, we believed that, in addition to transcriptional profiling, considering the hyperemia status of the tendon is essential for more comprehensive subtyping of tendinopathy.

Therefore, by combining transcriptome data with the macroscopic appearance of tendon color under arthroscopy, we further categorized tendinopathy into three subtypes, named Hw (Subtype H with white appearance), Iw (Subtype I with white appearance), and Ir (Subtype I with red appearance) (Fig. 1E). The heatmap illustrated the top 100 upregulated DEGs among the three subtypes and their associated top Gene Ontology biological process terms (Fig. 1F). The Venn diagram clearly illustrated DEGs that were specifically upregulated or downregulated in each of the three subtypes, as well as those commonly upregulated or downregulated genes (Fig. 1G, H). Enrichment analysis using Kyoto Encyclopedia of Genes and Genomes (KEGG) terms revealed that the pathways specifically upregulated in subtype Hw mainly included the HIF-1 pathway and several metabolic pathways, while in subtype Iw, it was Cytokine-cytokine receptor interaction, and in subtype Ir, they were mainly related to inflammation (Fig. 1I). The genes commonly altered in the three subtypes were enriched in metabolic and inflammatory pathways (Supplementary Fig. 3). In summary, subtype Hw was similar to Subtype H, primarily upregulating hypoxia and metabolic pathways. Subtype Iw and Ir were similar to Subtype I, mainly upregulating pathways related to inflammation. Subtype Ir exhibited the most pronounced inflammatory characteristics.

### Association of three distinct tendinopathy subtypes with clinical features

To understand the clinical characteristics of these biochemically and clinically-defined tendinopathy subtypes, we examined the differences in clinical features between these subtypes. There were no significant differences in age, biological sex ratio, height, weight, and course of the disease (Supplementary Fig. 4A–E). Figure 2A showed the ten most significant clinical features among the three subtypes, while Fig. 2B presented the top five clinically significant differences between each pair of the three subtypes (Fig. 2A, B). In the gross view under arthroscopy, subtype Ir exhibited the highest proportion of hyperemia in the tendon, glenohumeral synovium, and subacromial synovium (Supplementary Fig. 4F).

The Oxford shoulder score (OSS) in subtype Ir was the lowest, including the total score, and some items of the OSS (Fig. 2C and Supplementary Fig. 4G–M). The shoulder range of motion (ROM) in subtype Ir was the poorest, significantly lower in anteflexion, abduction, and external rotation compared to that in subtype Hw (Fig. 2D and Supplementary Fig. 4N–P). However, there were no significant differences in visual analogue scale (VAS) scores among the three subtypes (Supplementary Fig. 4Q, R). Regarding shoulder joint MRI, the coronal tear length was largest in subtype Ir, but there were no significant differences in the Patte stage or sagittal tear width (Supplementary Fig. 5A–C). The Goutallier stage was the highest in subtype Ir (Fig. 2E). No significant differences were found in the signal intensity ratios at these sites, including tendon stumps, normal tendon, supraspinatus muscle and armpit (Supplementary Fig. 5D–I). The shoulder joint examination and MRI results indicated that the joint function in subtype Ir was the worst.

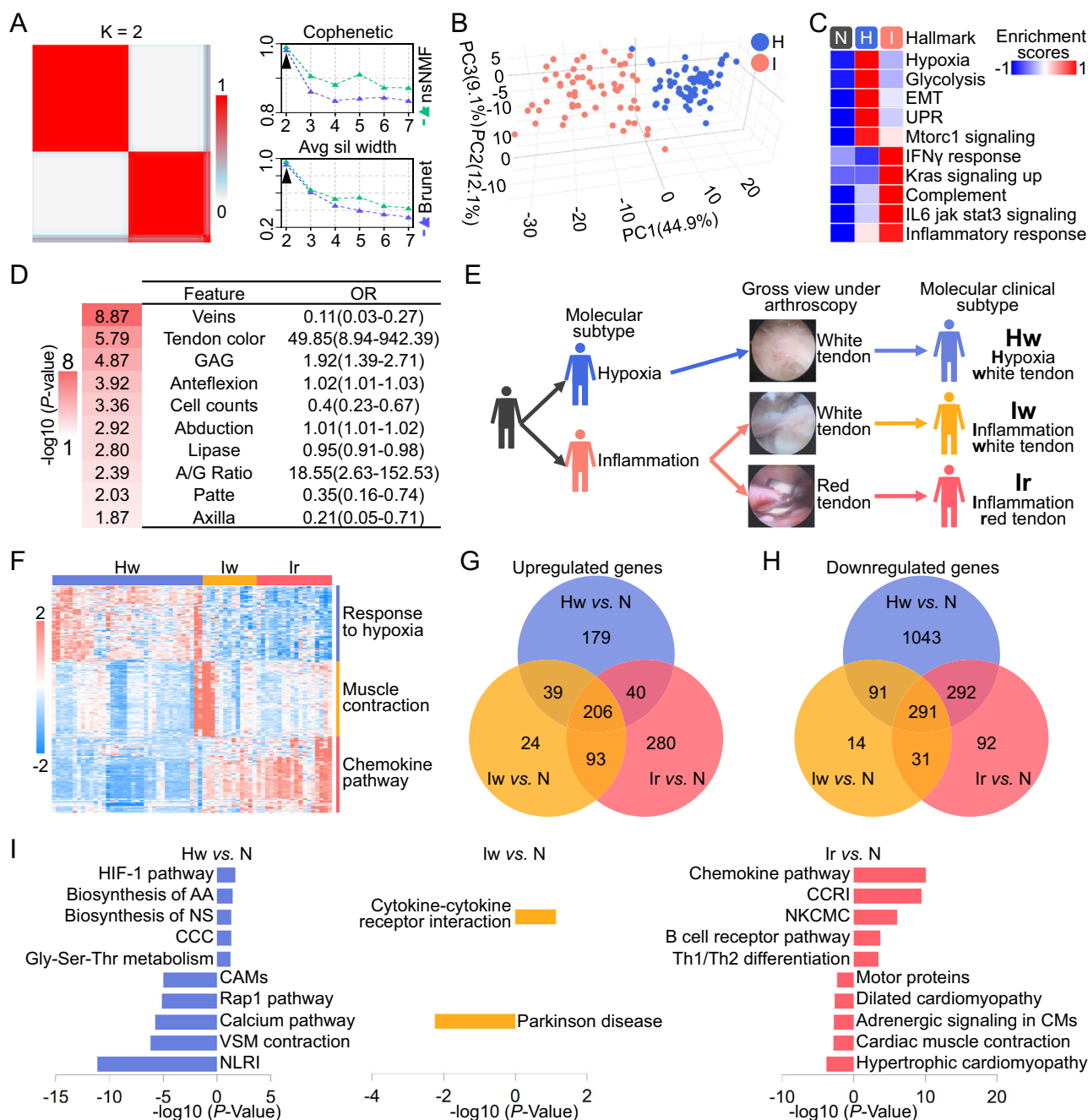


**Fig. 1 | Identification of three distinct subtypes of rotator cuff tendinopathy.**

**A** Heat map of NMF consensus matrix, cophenetic correlation coefficient and average silhouette-width plots. The green and blue points or lines in the cophenetic correlation and average silhouette-width plots represent the nsNMF and the Brunet algorithm, respectively. **B** Principal component analysis. First three principal components of RNA-seq data (Blue, Subtype H; Pink, Subtype I). **C** A heat map of alteration Hallmark pathways in the normal tendon, Subtype H and Subtype I. The color of each cell represents the average ssGSEA enrichment scores of that type; red denotes activation while blue denotes inhibition. (N, Normal tendon; H, Subtype H; I, Subtype I). **D** The top 10 clinical features with the most significant differences between Subtype H and Subtype I and their corresponding OR values. **E** Unsupervised clustering analysis identified two molecular subtypes of tendinopathy, further complemented by gross view under arthroscopy based on tendon color, resulting in the categorization of tendinopathy into three molecular clinical

subtypes. **F** The heat map depicted the relative abundance of DEGs in three tendinopathy subtypes. **G** Venn diagram of DEGs upregulated in each of the three tendinopathy subtypes compared to normal tendons. **H** Venn diagram of DEGs downregulated in each of the three tendinopathy subtypes compared to normal tendons. **I** Representative KEGG terms associated with genes that were specifically upregulated or downregulated in each subtype compared to normal tendons. The selection criteria for DEGs were a Log2 fold change  $> |2|$  with an adjusted  $P$  value  $< 0.01$ .  $P$  value of tendon color is calculated by Chi-Square Test.  $P$  values of other terms are calculated by the two-sided Mann-Whitney  $U$  test. EMT epithelial-mesenchymal transition, UPR unfolded protein response, AA amino acids, NS nucleotide sugars, CCC complement and coagulation cascades, CAMs cell adhesion molecules, VSM vascular smooth muscle, NLRI neuroactive ligand-receptor interaction, CCRI cytokine-cytokine receptor interaction, NKCMC natural killer cell-mediated cytotoxicity.



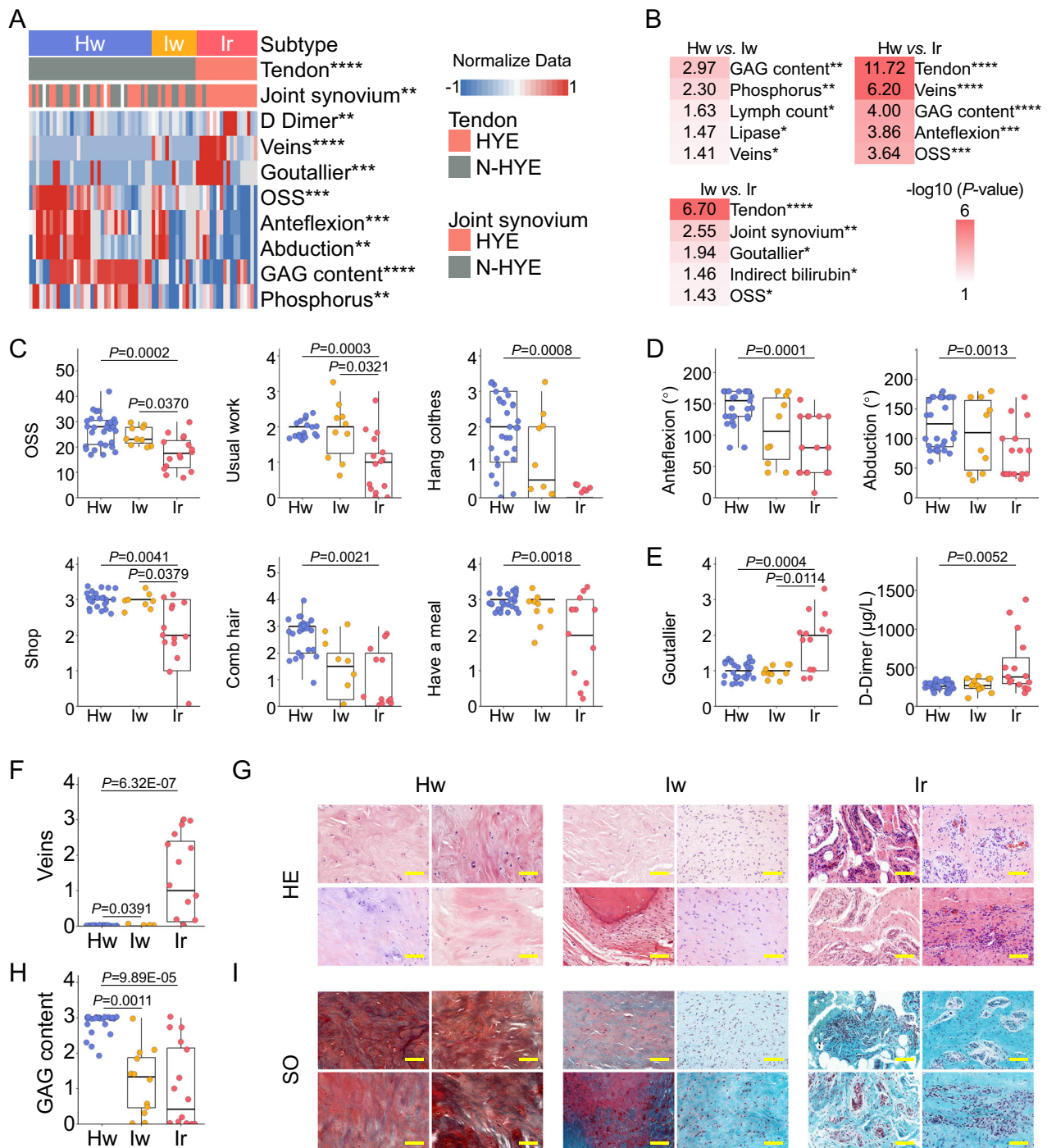


**Fig. 2 | Association of three distinct rotator cuff tendinopathy subtypes with clinical features.** **A** The association of the three tendinopathy subtypes with the top 10 clinical features with the most significant differences among the three subtypes (HYE, Hyperemia; N-HYE, Non-Hyperemia). **B** Top 5 clinical features with the most significant differences between Subtype Hw and Subtype lw, Subtype Hw and Subtype lr, as well as Subtype lw and Subtype lr. **C** Box plots of the total OSS, and selected items of the OSS, including usual work, hanging clothes, shopping, combing hair, and having a meal across the three tendinopathy subtypes (Hw,  $n=32$ ; lw,  $n=10$ ; lr,  $n=16$ ). **D** Box plots of the ROM for anteflexion and abduction in the affected shoulder joint across the three tendinopathy subtypes (Hw,  $n=30$ ; lw,  $n=10$ ; lr,  $n=17$ ). **E** Box plots of Goutallier stage (Hw,  $n=31$ ; lw,  $n=11$ ; lr,  $n=13$ ) and D-Dimer levels (Hw,  $n=30$ ; lw,  $n=11$ ; lr,  $n=16$ ) across the three tendinopathy subtypes. **F** Box plot of veins (one of the histological scores) across the three

tendinopathy subtypes (Hw,  $n=35$ ; lw,  $n=12$ ; lr,  $n=16$ ). **G** Representative HE images of diseased tendons from the three distinct tendinopathy subtypes. Scale bar: 100  $\mu$ m. **H**, Box plot of GAG content (one of the histological scores) across the three tendinopathy subtypes (Hw,  $n=35$ ; lw,  $n=12$ ; lr,  $n=16$ ). **I**, Representative SO images of diseased tendons from the three distinct tendinopathy subtypes. Scale bar: 100  $\mu$ m. The  $P$  values for tendon and joint synovium color was determined using the Corrected Chi-Square Test. The  $P$  values for phosphorus, lymph count, and OSS were calculated by ANOVA, while other terms were analyzed using the two-sided Kruskal–Wallis test. In the box plots, the middle line represents the median, with the box denoting the interquartile range; whiskers extend to 1.5 $\times$  the interquartile range. Source data are available in the Source Data file. OSS Oxford Shoulder Score, GAG glycosaminoglycan.

With regards to blood testing, the three distinct subtypes also exhibited differences, particularly in coagulation function. The results showed that subtype Ir had significantly higher levels than subtype Hw in D-Dimer, Prothrombin Time, and International Normalized Ratio (Fig. 2E and Supplementary Fig. 6A, B). PT activity in subtype Ir was significantly lower than that in subtype Hw (Supplementary Fig. 6C). The examination results of coagulation function indicated that patients with subtype Ir might have thrombosis or that their blood was in a hypercoagulable state.

The serum phosphorus concentration in subtype Hw was significantly higher than that in subtype Iw (Supplementary Fig. 7A). Other results for blood electrolytes (Supplementary Fig. 7B–F), renal function (Supplementary Fig. 7G–L), and lipid levels (Supplementary Fig. 7M–S) showed no significant differences. Regarding liver function indicators, subtype Hw exhibited significantly higher levels of albumin, beta-hydroxybutyrate, and glycyl-proline-dipeptidyl aminopeptidase compared to subtype Ir (Supplementary Fig. 8A–C), while subtype Iw showed significantly higher levels of indirect bilirubin compared to subtype Ir (Supplementary Fig. 8D). The lipase level in subtype Hw was significantly lower than that in subtype Iw (Supplementary Fig. 8E). In terms of routine blood parameters, the lymphocyte count in subtype Hw was significantly higher than that in subtype Iw (Supplementary Fig. 9).

Histologically, subtype Ir had the highest scores for the veins (Fig. 2F, G), while the tissue in subtype Hw showed a significantly higher proportion of red-stained areas in the SO staining results, indicating a higher glycosaminoglycan (GAG) content (Fig. 2H, I). Other histological scores did not show significant differences among the three subtypes (Supplementary Fig. 10). It can be observed that the hyperemia features in subtype Ir were consistent both histologically and macroscopically, while the large red area in the SO staining results in subtype Hw also suggested the possibility of its chondrification.

In summary, the shoulder joint function of subtype Ir was the worst. The differential manifestations of vascular features among the three subtypes might be a crucial mechanism underlying the occurrence of these subtypes.

### Key pathogenic mechanisms and key regulatory genes of the three distinct rotator cuff tendinopathy subtypes

To gain a better understanding of the functional differences between tendinopathy subtypes, we applied gene set variation analysis (GSVA) from the molecular signature database (MSigDB) using hallmark pathways (Supplementary Fig. 11). Subtype Hw significantly upregulated pathways, such as Hypoxia and Glycolysis. Both the Iw and Ir subtypes exhibit upregulated signaling pathways related to inflammation. GSEA plots delineate specific differences among the three subtypes. The neovascularization pathway was significantly downregulated in subtype Hw, while subtype Ir exhibited a significant upregulation, consistent with the intraoperative appearance and histological findings (Fig. 3A and Supplementary Fig. 12A). Subtype Hw showed a significant upregulation of pathways, such as hypoxia (Fig. 3B and Supplementary Fig. 12B), glycolysis, Cori cycle, chondrocyte differentiation, and cartilage development (Supplementary Fig. 12C–F and Supplementary Fig. 13A–D). There was a significant upregulation of inflammatory-related pathways in subtypes Iw and Ir (Fig. 3C and Supplementary Fig. 13F–H). Subtype Ir exhibited more inflammatory-related features than subtype Iw (Supplementary Fig. 12G–K). Additionally, subtype Hw showed a significant downregulation of the endothelial cell proliferation pathway, while subtype Ir exhibited a significant upregulation of this pathway (Supplementary Fig. 12L and Supplementary Fig. 13I).

Multi-scale embedded gene coexpression network analysis (MEGENA) was utilized to identify potential key regulators of the molecular changes in each subtype. A total of 108 modules with a module size >100 were identified from our dataset using MEGENA

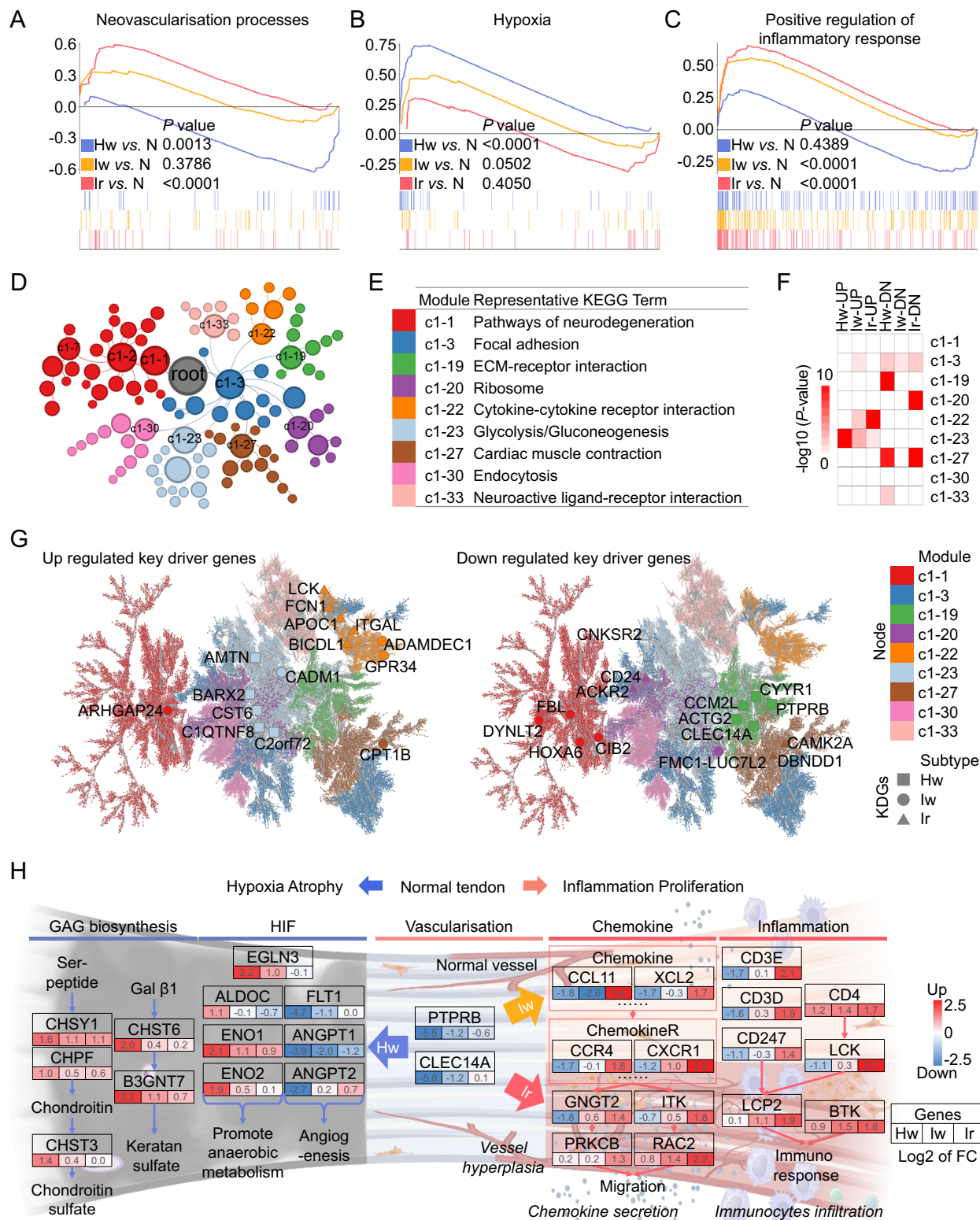
(Fig. 3D). Major modules were annotated by significantly associated KEGG terms (Fig. 3E). The module most correlated with the upregulated gene set in subtype Hw was c1-23, with the representative KEGG term being Glycolysis/Gluconeogenesis. For subtype Ir, the module was c1-22, with the representative KEGG pathway being Cytokine-cytokine receptor interaction. In the downregulated gene set, the modules most correlated with subtype Hw were c1-19 and c1-27, while those most correlated with subtype Ir were c1-20 and c1-27 (Fig. 3F). Figure 3G illustrated the up- and down-regulated key drivers of each subtype in the context of the MEGENA network (Fig. 3G). The top 5 specifically upregulated key driver genes (KDGs) in subtype Ir were primarily associated with inflammatory pathways and belonged to c1-22. The top 5 specifically upregulated KDGs in subtype Hw all belonged to c1-23. The top 5 specifically upregulated KDGs in subtype Iw belonged to multiple modules. Among the top 5 specifically downregulated KDGs in subtype Hw all belonged to c1-19. It had been reported before that both C-Type Lectin Domain Containing 14A (CLEC14A) and Protein Tyrosine Phosphatase Receptor Type B (PTPRB) were associated with angiogenesis.

In summary, the primary molecular features of subtype Hw included a significant upregulation of the hypoxia pathway and chondrogenic-related GAG synthesis pathways due to the downregulation of the angiogenesis pathway. Consequently, we also termed subtype Hw as the hypoxic atrophic subtype. In contrast, the angiogenesis pathway in subtype Ir was significantly upregulated, which was evident from the substantial infiltration of blood vessels observed both arthroscopically and histologically. This is accompanied by the highest level of inflammation and chemotactic features among the three subtypes. Subtype Iw did not exhibit significant infiltration of blood vessels, and its inflammation level was much lower than that of subtype Ir. Therefore, we referred to subtype Iw as the intermediate inflammatory proliferative subtype, while subtype Ir was referred to as the high inflammatory proliferative subtype (Fig. 3H).

### Tendinopathy subtypes translated to animal models uncover the potential for personalized therapy

This part of the study aimed to establish a transcriptomic database of animal models for tendinopathy, providing representative animal models for different clinical subtypes and exploring precision therapeutic strategies for different tendinopathy subtypes. The schematic diagram briefly described the process of screening, establishment, validation, and subtype prediction (Fig. 4A). Initially, we predicted induction mechanisms of specific tendinopathy subtypes based on the molecular data of tendinopathy. De-redundant annotation clustering identified inflammatory response and oxidative stress as critical inducers for the Ir subtype, while hypoxia and collagen degradation were identified as key inducers for the Hw subtype (Supplementary Fig. 14). We conducted a systematic review of animal models of tendinopathy and selected those that matched the anticipated mechanisms<sup>17</sup>: PGE2 model for inflammatory response, levofloxacin model for oxidative stress, ligation model for hypoxia, and collagenase model for collagen degradation. In addition to models chosen based on molecular characteristics, we also constructed a forced-running model.

We conducted detailed transcriptomic and histological characterization of five models. The ligation, collagenase, levofloxacin, and PGE2 models successfully replicated the histopathological manifestations of tendinopathy (Supplementary Figs. 15–18). The treadmill running model did not exhibit tendinopathy characteristics at the molecular pathological level (Supplementary Fig. 19). Transcriptomic enrichment analysis indicated that molecular characteristics of the levofloxacin and PGE2 models are primarily associated with inflammation and immunity, while those of the ligation and collagenase models relate to extracellular matrix organization and anatomical structure development (Supplementary Figs. 15–18).



We then explored the intrinsic heterogeneity of tendinopathy animal models through unsupervised clustering using NMF. NMF analysis revealed that the animal models exhibited heterogeneity and were best suited for categorization into two subtypes (Supplementary Fig. 20A, B). One subtype comprised the levofloxacin model and PGE<sub>2</sub> model, while the other subtype comprised the ligation model and collagenase model (Supplementary Fig. 20C). We conducted subtype determination of animal models based on characteristic genes using NTP. The collagenase model was classified as Hw, while the other

models were classified as Ir (Fig. 4B). GSVA analysis showed that proliferation, chemotaxis, and inflammation-related pathways were enriched in the levofloxacin, PGE<sub>2</sub>, and ligation models, while hypoxia, metabolism, and chondrocyte-related pathways were enriched in the ligation and collagenase models (Fig. 4B).

We conducted a more in-depth review of the advantages and disadvantages of each animal model in replicating subtypes by using cross-species integrative analysis. From the perspective of subtype proximity, the molecular spectra of the levofloxacin and collagenase



**Fig. 3 | Key pathogenesis and key regulatory genes of the three distinct rotator cuff tendinopathy subtypes.** **A–C** GSEA revealed altered pathways (WP NEO-VASCULARISATION PROCESSES, FARDIN HYPOXIA 11, GOBP POSITIVE REGULATION OF INFLAMMATORY RESPONSE) between the three distinct tendinopathy subtypes and normal tendons. (Blue, Hw vs. N; Yellow, Iw vs. N; Red, Ir vs. N). **D** A global MEGENA network. The main modules and their sub-modules are represented in the same color. **E** Representative KEGG pathways associated with the MEGENA modules. **F** GeneOverlap analysis was conducted to ascertain the correlation between different MEGENA modules and various gene sets, which encompassed genes that were either upregulated or downregulated in each of the different subtypes compared to normal tendons. **G** Top up- and down-regulated MEGENA

key drivers for each subtype plotted in its location in the network. Each point represents a gene. Points of different colors represent different gene co-expression modules. (KDGs, key driver genes). **H** Biological insight into the three distinct tendinopathy subtypes. The diagram summarized relevant signatures and signaling cascades involved in the HIF signaling pathway, GAG biosynthesis in Subtype Hw and chemokine, and inflammation pathway in Subtype Iw and Ir. Alterations were defined by up- or downregulation of genes. Alteration scores of each gene are depicted as log ratios (fold change, expressed as log<sub>2</sub> (ratio of average gene abundance in each transcriptomic subtype versus the normal tendon group)). Red, upregulated genes; blue, downregulated genes.

models were closest to the human Ir and Hw subtypes, respectively. The integrative analysis captured signature immune-related pathways of Subtype Ir in the levofloxacin model, such as immune system development and abnormal immune system morphology (Supplementary Fig. 21, pathway 4 and 11). Additionally, the levofloxacin model manifested several molecular features of Subtype Ir tendinopathy like abnormal vascular morphology, and responses to oxidative stress (Supplementary Fig. 21, pathway 1 and 5). The collagenase model summarized the ossification-related pathways of the Hw subtype tendinopathy, such as skeletal system development and abnormal upper limb bone morphology (Supplementary Fig. 22, pathway 1 and 12). Moreover, collagen containing extracellular matrix and apoptotic signaling pathway (Supplementary Fig. 22, pathway 8 and 10) were co-enriched in both the collagenase model and Hw subtype tendinopathy.

Subsequently, we investigated the therapeutic properties of glucocorticoids on the representative models. Glucocorticoids significantly improved the histological scores of the levofloxacin models (Fig. 4C, D). After glucocorticoid therapy, large collagen fibers (collagen diameter >100 nm) were observed only in the levofloxacin group (Fig. 4E, F). Furthermore, behavioral assessment through treadmill running experiments showed a significant improvement only in the levofloxacin group (Fig. 4G and Supplementary Movie. 1,2). The GSVA analysis showed that glucocorticoids can effectively reverse the inflammatory characteristics of the Ir subtype of tendinopathy (Fig. 4I). Additionally, in the scenario of laceration repair, we reassessed the efficacy of glucocorticoids on the representative model. The results similarly support that glucocorticoids have a more beneficial effect on the Ir subtype of tendinopathy in animal models (Fig. 4C, E and Supplementary Fig. 23).

We then explored the mechanistic effects of glucocorticoids on the Ir subtype tendinopathy from the perspectives of protein interaction and transcriptional regulation. Based on molecular data from clinical Ir subtype patients and in vivo experiments, we screened proteins that play an active role in reversing the molecular characteristics of the Ir subtype under glucocorticoid treatment (Fig. 4H). Glucocorticoids can regulate blood vessel development through FOSB and FOSL1, and neutrophil activation via CCL5 and FCER1G. Starting from transcriptional regulation, we identified individual regulators whose target genes have a significant overlap with the key target genes of subtype Ir, levofloxacin, and glucocorticoid therapy. In the levofloxacin model following glucocorticoid treatment, 25 co-enriched transcriptional regulators were reversed, and the enrichment analysis suggests that the efficacy of the glucocorticoids is associated with the PPAR signaling pathway, Wnt Signaling Pathway, and TNF-alpha NF-kB Signaling Pathway (Fig. 4J).

Our results thus indicate that animal models induced by different mechanisms can to some extent differentially manifest the various characteristics of tendinopathy subtypes. Glucocorticoid treatments are more effective in animal models that match the high inflammatory proliferative subtype, leading to enhanced healing of injured tendons.

## Clinical data to verify the therapeutic effects of glucocorticoids on different tendinopathy subtypes

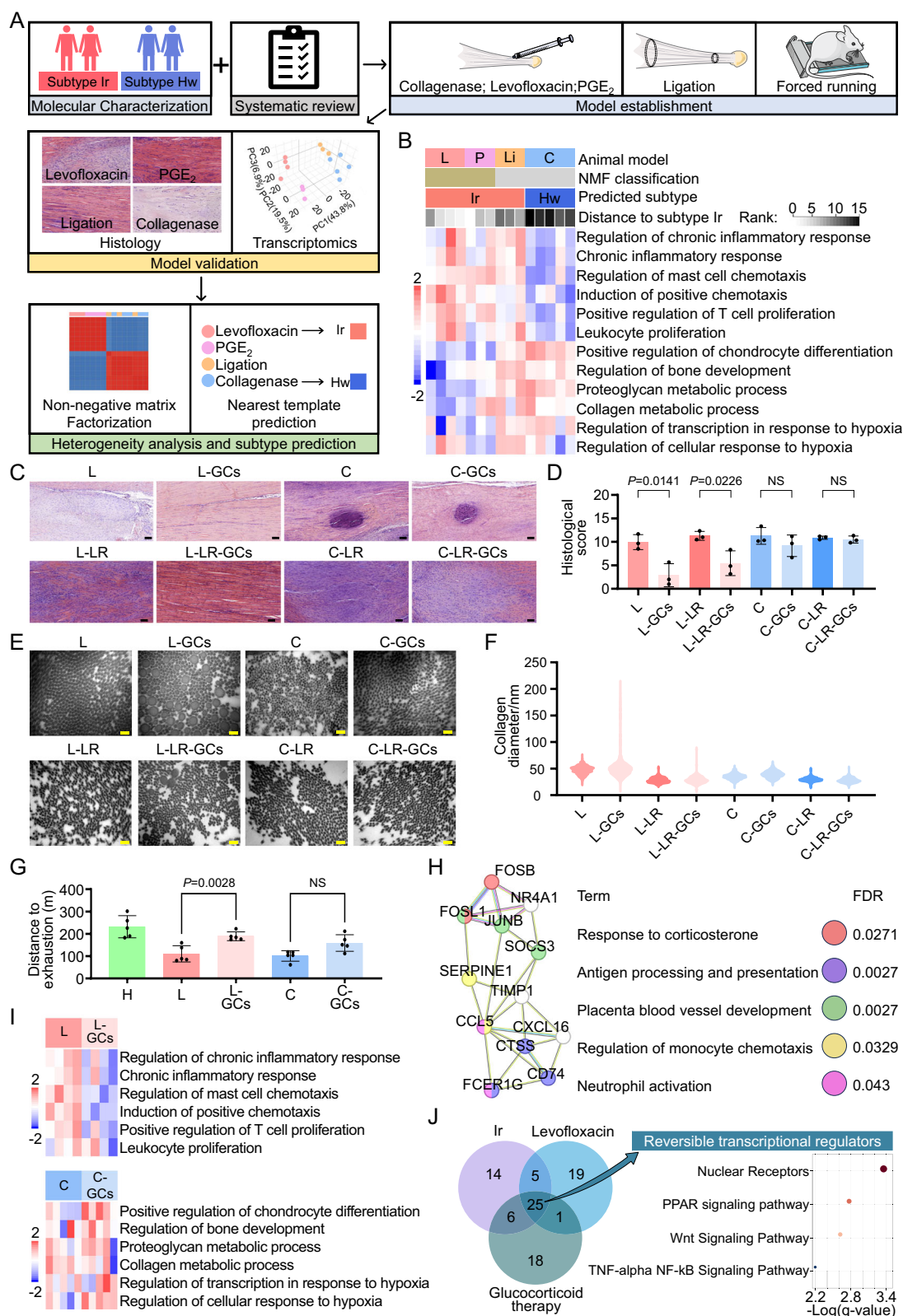
We further compared the differences in prognostic improvement among patients with different tendinopathy subtypes who underwent intraoperative glucocorticoid administration. Our patients received local glucocorticoid injections based on conventional surgical sutures, and we conducted follow-ups on these patients. The disparities in the improvement of shoulder joint range of motion, pain scores, and OSS between patients with different subtypes at 6 months and 24 months post-surgery were compared. At 6 months and 24 months post-surgery, the improvements in anteflexion and abduction in subtype Ir were significantly better than those in subtype Hw (Supplementary Data. 1,2). Analyzing the OSS items at 6 months post-surgery, we found that in subtype Ir, the improvement in the item of comb hair was significantly greater than that in subtype Hw (Supplementary Data. 1). This clinical study further confirmed that glucocorticoid therapy was only effective for the high inflammatory proliferative subtype.

## Discussion

In this study, we proposed that rotator cuff tendinopathy with moderate tear can be classified into three distinct subtypes with completely different pathological mechanisms. Subtype Hw exhibited downregulation of the neovascularization pathway and upregulation of HIF, glycolysis, and cartilage-associated signaling pathways. Conversely, subtype Ir exhibited a significant upregulation of the neovascularization and inflammation pathways, with substantial vascular infiltration. There was no significant vascular infiltration in subtype Iw, which displayed only a moderate increase in inflammatory proliferation features. Our results thus indicated that a single pathological mechanism was insufficient to fully explain the complexity of tendinopathy. Multiple hypotheses have been previously proposed regarding the pathogenesis of tendinopathy, including inflammation theory, apoptosis theory, mechanical theory, and vascular and neurogenic theory<sup>1</sup>. Based on our research findings, it turned out that several debatable conditions indeed coexist in tendinopathy, thus providing a crucial theoretical foundation for precision treatments in the future.

Imaging is an important diagnostic tool for evaluating the severity of tendon pathology<sup>18</sup>. Using magnetic resonance imaging, the diseased tendons were classified based on tear size, degree of tendon retraction, and extent of fatty infiltration<sup>18</sup>. Although subtype Ir exhibited the greatest tear length and highest Goutallier stage, the differences in these MRI features were not sufficient to identify subtypes of tendinopathy based solely on this data. Artificial intelligence has been used to extract MRI features in bulk for subtype diagnosis in various diseases<sup>19,20</sup>. In the future, this technology can be explored to find predictive diagnostic methods for tendinopathy subtypes.

The incidence of hyperlipidemia in our cohort of tendinopathy patients (59.8%) is higher than the reported incidence in the general population (34.0%)<sup>21</sup>. This is consistent with previous studies showing that hyperlipidemia can promote the development of tendinopathy<sup>22</sup>. However, the lipid-related data we collected did not show significant differences among the three subtypes. This suggests that changes in



lipid levels may not be a key factor in the formation of any specific tendinopathy subtype.

The model induced by levofloxacin, one of the fluoroquinolones, is considered a typical subtype Ir model. Clinical data revealed an increased incidence of tendon injury upon treatment with fluoroquinolone<sup>23</sup>. The mechanism for tendinopathy induced

by levofloxacin is oxidative stress<sup>23</sup>, which can activate a variety of transcription factors, leading to the differential expression of genes involved in inflammatory pathways<sup>24</sup>. Our results indicated that the levofloxacin model upregulated a significant number of pathways related to inflammation. These upregulated pathways coincided with those elevated in the human tendinopathy subtype Ir.



**Fig. 4 | The therapeutic effects of glucocorticoid therapy on animal models of the different tendinopathy subtypes.** **A** Schematic workflow for the establishment of animal models for the different subtypes of tendinopathy. **B** GSVA identified clinical subtype characteristics recapitulated by animal models. Model classification based on induction methods, NMF grouping, nearest template prediction, and subtype Ir proximity is shown at the top. The heatmap displays GSVA Z scores of subtype-signature biological processes (rows) across tendinopathy models (columns). **C** Hematoxylin and eosin staining of tendons after glucocorticoid treatment. Scale bar: 50  $\mu$ m. **D** Histological evaluation of each group. **E**, Representative TEM images of each group ( $n = 3$ ). Scale bars: 0.2  $\mu$ m. **F** Quantitative diameters of the collagen fibrils. **G** Running distance of each group during the run-to-exhaustion test. **H** Defining protein-protein interaction network of glucocorticoid-reversible Ir key genes. The functional network was constructed from 12 key proteins according to node degree. Edges indicated both functional and physical protein associations, and their thickness indicated the strength of data support. **I** GSVA revealed changes in subtype characteristics of the animal model after glucocorticoid treatment. Heatmap depicts GSVA standardized score (Z

score) of subtype-signature biological processes (row) in the tendinopathy model (column). **J** Differentially expressed genes (Subtype Ir and normal human tendon; Levofloxacin and normal rat tendon; Levofloxacin and Levofloxacin after glucocorticoid treatment) were used for over-representation analysis to identify key transcriptional regulators. Enrichment analysis was conducted for 25 glucocorticoid-reversed concurrently enriched transcriptional regulators. Independent data points represent biological replicates. Bar charts show mean values with error bars indicating SD. *P* values were calculated using the two-sided Student's *t* test, with NS for  $P > 0.05$ . Source data are provided in the Source Data file. L levofloxacin model, P PGE2 model, Li ligation model, C collagenase model, L-GCs levofloxacin model with glucocorticoid treatment, L-LR levofloxacin model in the scenario of laceration repair, L-LR-GCs levofloxacin model with glucocorticoid treatment in the scenario of laceration repair, C-GCs collagenase model with glucocorticoid treatment, C-LR collagenase model within the scenario of laceration repair, C-LR-GCs collagenase model with glucocorticoid treatment in the scenario of laceration repair.

Additionally, it has also been reported that steroid therapy mitigated fluoroquinolone-induced oxidative stress<sup>25</sup>.

The collagenase model is considered a typical Hw subtype model. Collagenase injection degrades the tendon matrix, resulting in disrupted collagen structure, but increased chondrogenic and osteogenic gene expression, together with calcium deposition<sup>17</sup>. Our results demonstrated that the collagenase model shared similar molecular characteristics with the subtype Hw, particularly in jointly upregulating pathways related to cartilage differentiation. The compromised microvascular structure, endothelial injury, and increased hypoxia may be crucial factors leading to tendon calcification<sup>26</sup>. Intratendon delivery of leukocyte-poor platelet-rich plasma can significantly promote the healing of collagenase models<sup>27</sup>. Adipose-derived stem cells can induce neovascularization in collagenase-induced models, promoting tendon repair and preventing ectopic ossification<sup>28</sup>.

Overuse is one of the primary causes of tendinopathy, and the overuse model is a valuable animal model for simulating tendinopathy<sup>1</sup>. However, according to our results, other modeling approaches more closely resemble the patient sample scenario. This may be because our samples were predominantly from severely diseased tendon specimens. Perhaps overuse model is better suited for simulating less severe tendon pathologies.

Multiple treatment strategies operate through different mechanisms. Based on the molecular characteristics of the three subtypes of tendinopathy and combining mechanisms of action from previous studies, we thus propose potential treatment approaches for these subtypes. For example, the scientific literature suggests that ultrasound<sup>29</sup> and ESWT<sup>30</sup> promote blood flow perfusion, while PRP facilitates angiogenesis<sup>31</sup>. Stem cell therapy is well-attested to enhance local tissue repair<sup>32</sup>. The primary feature of the Hw subtype is hypoxic atrophy, so these regenerative treatments<sup>29–32</sup> could be preferred for patients with hypoxic atrophy. Additionally, studies have demonstrated that PRP has anti-inflammatory effects<sup>31</sup>. The Ir subtype is characterized by a moderate increase in inflammation levels, so we recommend considering anti-inflammatory therapies and regenerative approaches<sup>31,32</sup> when treating the Ir subtype. For the Ir subtype, which exhibits the most inflammatory and proliferative molecular characteristics, anti-inflammatory treatments are recommended. Our experimental data across two levels—animal models and clinical data—consistently demonstrate the effectiveness of glucocorticoids in treating the Ir subtype.

The effectiveness of glucocorticoids in the treatment of tendinopathy is controversial. It has been reported that using glucocorticoids can alleviate pain, improve sleep quality, and facilitate functional shoulder exercise<sup>33</sup>. Intra-articular injection of glucocorticoids after rotator cuff repair did not increase the risk of retear and was an effective and safe treatment method for increasing ROM<sup>9</sup>. However, in

some studies, glucocorticoid therapy did not yield a more significant improvement in prognosis<sup>5,34</sup> and even showed adverse effects<sup>35</sup>, such as decreasing cell viability, increasing cell apoptosis<sup>36</sup>, damaging histological structure and weakening mechanical properties<sup>37</sup>.

Our preclinical experiments had shown that glucocorticoids were effective for levofloxacin-induced models but harmful for collagenase-induced models. The clinical results also confirmed the heterogeneity of glucocorticoid efficacy. Glucocorticoids can suppress inflammation in subtype Ir, but subtype Hw did not exhibit significantly elevated inflammatory characteristics. The use of glucocorticoids cannot exert its anti-inflammatory effects on subtype Hw, leaving only side effects<sup>9</sup>. In our study, the proportion of subtype Hw was 53.7%. Previous studies had debated the effectiveness of glucocorticoid therapy, possibly due to issues in the selection of the target population, including patients with subtype Hw who should not receive glucocorticoid treatment. Selecting patients with specific subtypes for clinical research and targeting the underlying mechanisms could be a crucial direction for future clinical studies on tendinopathy.

Several limitations exist in this study. One of these is the lack of matching control samples. An ideal control for this current study would be a matched number of healthy supraspinatus tendon samples, but practically speaking, the opportunity to collect these samples without impacting patients' well-being is challenging. Animal models have limitations in fully replicating human tendinopathy subtypes. Despite differences between animal models and humans, they provide a critical tool for scientific research, offering foundational data and experimental validation in the search for treatments for tendinopathy.

In summary, we have systematically identified three distinct subtypes of tendinopathy and subsequently characterized their molecular signatures, network regulatory genes, and clinical features (Fig. 5). This offers an opportunity to expedite the translation of basic research into more precise diagnosis and treatment in the clinic. It is anticipated that the one size fits all treatment strategy will eventually shift to a subtype-based treatment approach.

## Methods

### Patient data

This research complies with the ethical regulations for work with human tissue samples and medical history, and for animal studies. The patient's written consent and approval of the local ethics committee were obtained (Ethics Committee of the second Affiliated Hospital, School of Medicine, Zhejiang University, code: 2019-168, 2020-080). The animal work was approved by the Zhejiang University Institutional Animal Care and Use Committee (ZJU20220006).

The inclusion criteria were patients with confirmed supraspinatus tendon injuries based on MRI, with tear lengths less than 5 cm. Patients with massive rotator cuff tears larger than 5 cm were excluded. The

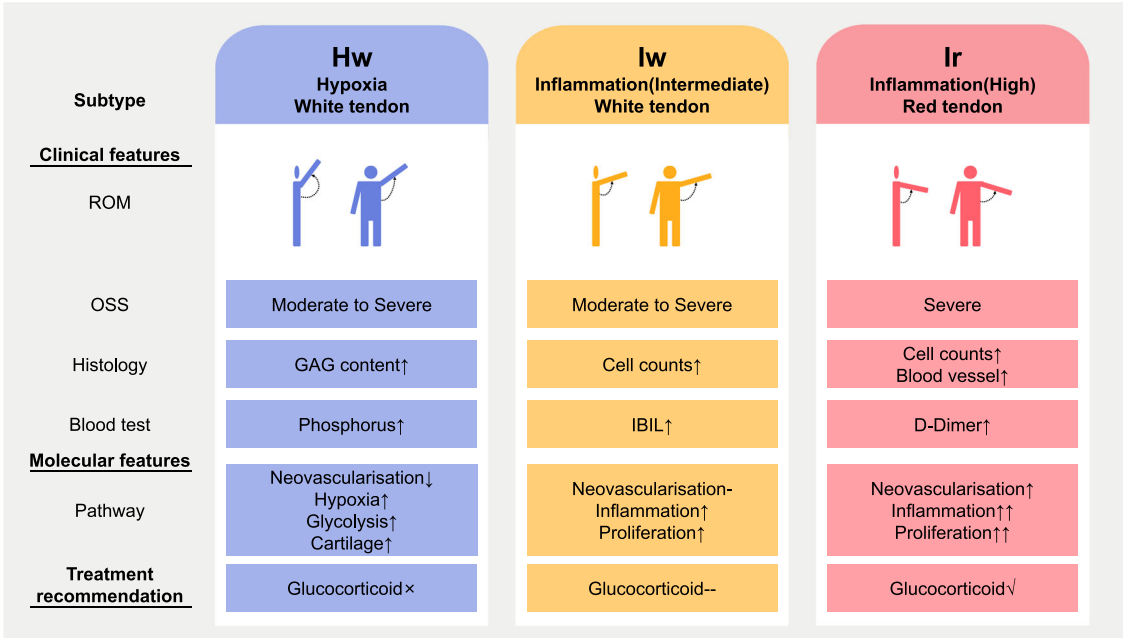


**Fig. 5 | Summary of characteristics of the three distinct rotator cuff tendinopathy subtypes.** The major clinical features, molecular features and treatment recommendation of three distinct rotator cuff tendinopathy subtypes are summarized. The clinical features mainly include the ROM of the shoulder joint before surgery, OSS, histology, and results of blood tests. Molecular features focus on the

signal pathways with characteristic changes. The treatment recommendation is primarily directed towards specific subtypes of patients who are suitable for glucocorticoid therapy. ROM range of motion, OSS Oxford shoulder score, GAG glycosaminoglycan, IBIL indirect bilirubin.

human-diseased tendon samples were surgical waste obtained during arthroscopic shoulder surgery ( $n = 126$ ). Healthy hamstring tendons were collected from patients undergoing surgical reconstruction of their anterior cruciate ligament ( $n = 28$ ). The clinical profiles for each participant were also collected including basic clinical information, magnetic resonance imaging data, joint range of motion, oxford shoulder score, VAS score at rest and after activity, status of tendon and synovium under arthroscopy, and blood testing. Basic clinical information typically included age, gender ratio, height, weight, and course of disease. The range of motion of the shoulder joint included anteflexion, abduction, external rotation, and internal rotation. We assessed the condition of the tendon and synovium under arthroscopy, distinguishing between red hyperemia and white non-hyperemia. Blood tests comprised commonly utilized clinical assessments, including coagulation function, electrolytes, renal function, lipid profile, liver function, kidney function, and other routine blood assays.

**RNA sequence**

Total RNA was extracted from the tissue using TRIzol® Reagent according to the manufacturer's instructions (Invitrogen) and genomic DNA was removed using DNase I (Takara). RNA-seq transcriptome libraries were prepared with the TruSeq™ RNA sample preparation Kit from Illumina (San Diego, CA), using 1 µg of total RNA. Briefly, messenger RNA was isolated with polyA selection by oligo(dT) beads and fragmented using a fragmentation buffer. cDNA synthesis, end repair, A-base addition, and ligation of the Illumina-indexed adaptors were performed according to Illumina's protocol. Libraries were then size-selected for cDNA target fragments of 200–300 bp upon electrophoresis on 2% (w/v) Low Range Ultra Agarose, followed by PCR amplification using Phusion DNA polymerase (NEB) for 15 PCR cycles. After quantification by TBS380, Paired-end libraries were sequenced with the Illumina HiSeq PE 2X150bp read length.

**Reads quality control and mapping**

The raw paired-end reads were trimmed and quality-controlled by Trimmomatic with default parameters (<http://www.usadellab.org/cms/uploads/supplementary/Trimmomatic>). Then clean reads were separately aligned to the reference genome with orientation mode using hisat2 (<https://ccb.jhu.edu/software/hisat2/index.shtml>) software<sup>38</sup>. Tophat was a program that can align RNA-Seq reads to a genome to identify gene expression and exon-exon splice junctions. It is built on the ultrafast short-read mapping program Bowtie2. This software was used to map with default parameters.

**Clustering of RNA-seq data**

To account for any batch effects, we used the remove batch effect function in the bioconductor limma package and DESeq2 (v.1.36.0) to normalize the data. The top 2000 most-variant genes were subjected to non-negative matrix factorization (NMF) (v.0.24.0) for unsupervised consensus-clustering. The non-smooth NMF (nsNMF) and the Brunet algorithm were performed using 400 iterations for the rank survey and clustering runs<sup>39,40</sup>. A preferred cluster result was selected by considering the profiles of the cophenetic score and average silhouette width for clustering solutions between 2 and 7 clusters. The rank survey profiles of the cophenetic score and silhouette width—along with the consensus membership heat maps—indicated a two-subtype solution for tendinopathy using the RNA-seq data.

**Classification based on transcriptomic and clinical data**

Based on the NMF classification, we further categorized samples by the presence of a red hyperemia state in tendons observed under arthroscopy. Samples lacking arthroscopic data were excluded from subsequent analyses. Since there was only one red hyperemia tendon in the subtype H, it was not included in further analyses. White tendons in the subtype H were defined as the subtype Hw ( $n = 36$ ). In the subtype I, white tendons were defined as the subtype lw ( $n = 13$ ), and red hyperemia tendons were defined as the subtype lr ( $n = 18$ ).

## Differential gene expression analysis and enrichment analysis

We used the DESeq2 Bioconductor package<sup>41</sup> to identify DEGs across normal tendon and tendinopathy subtypes that were identified via clustering. Gene Ontology (GO) and Kyoto Encyclopedia of Genes and Genomes (KEGG) pathway enrichment analysis were performed using DAVID. Gene set enrichment analysis (GSEA) was completed through GSEA software (<http://www.gsea-msigdb.org/gsea/index.jsp>) (v.4.1.0). We performed gene set variation analysis (GSVA) to identify the pathway alterations that underlie our subtypes, using the R/Bioconductor package GSVA (v.1.44.5)<sup>42</sup>. To deconvolute the cellular composition of the two tendinopathy subtypes and normal tendons in our data, we used an algorithm called xCell (v.1.1.0), a powerful machine learning framework trained on the profiles of immune and stroma cell datasets, for generating cell type enrichment scores and adjusting them to cell type proportions<sup>43</sup>.

## Network construction and key regulator identification

A multiscale embedded gene expression network analysis (MEGENA) (v.1.3.7) network was generated from our RNA-seq data<sup>44</sup>. We used Gephi to generate a connectivity graph of sub-modules within all modules. We conducted KEGG enrichment analysis separately for all genes within each module. The R package GeneOverlap (v.1.32.0) was employed to analyze the correlation between different modules and sets of DEGs. Then we performed key driver analysis (KDA) (v.0.2.2) on the MEGENA network to identify key hub genes that regulated a large number of downstream nodes<sup>45</sup>. The interaction diagram between modules was created using Gephi (v.0.10.1). The network interaction diagram was generated using Cytoscape (v.3.9.1).

## Histological analysis and scoring

The isolated human normal and diseased tendons were processed for histological analysis. First, tissues were fixed in 4% (w/v) paraformaldehyde for 24 h. After dehydration with graded ethanol, clearing and wax immersion, the samples were embedded in paraffin blocks. The sections (7 µm) were then prepared using a microtome, subsequently stained with H&E and Safranin O, and eventually photographed under a microscope (Pannoramic MIDI, 3DHISTECH). The histological score was performed based on H&E and Safranin O staining according to the scoring system that was modified from a previous study<sup>46,47</sup>. Briefly, the eight parameters (fiber structure and arrangement, cell population, roundness of nuclei, inflammation, vascularity, hyalinization, and GAG content) were semi-quantitatively assessed with a score range of 0–24. Lower scores indicate better tissue quality.

## MRI signal values measurement

Participants underwent a standardized imaging protocol using a Magnetom Essenza MRI with a field strength of 1.5 T. The tear size was determined by preoperative MRI at the coronal and sagittal position and Patte staging was used to evaluate the tendon retraction<sup>48</sup>. We also assessed fatty degeneration of the rotator cuff muscles with preoperative MRI using Goutallier staging<sup>48</sup>. On the T2 fat SAT fat-suppressed imaging with the largest rotator cuff tear, the signal intensities in 10-mm<sup>2</sup> circles at these points were measured (Weasis, v.3.5.3), including three consecutive tendon stumps, normal tendon, supraspinatus muscle, axillary and deltoid muscle (Supplementary Fig. 24). Taking the deltoid signal values as the reference, the ratio of other parts of the signal values to the deltoid signal values was calculated<sup>49</sup>.

## Construction of animal tendinopathy models

We used 8 weeks old male Sprague-Dawley adult rats with a body weight ranging from 230 to 270 g to create tendinopathy models in this study. A total of 5 rats were included as the normal control. 25 rats (50 tendon samples) were assigned to the 5 tendinopathy models, as described in Supplementary Data 3. Explanted tendon samples were

subjected to transcriptomic sequencing and histological evaluation following euthanasia with excess pentobarbital sodium at the designated time point.

## Construction of the laceration repair model

All surgical procedures applied to the rats were performed after controlling the pedal reflex under general anesthesia (intraperitoneal injection of 40 mg/kg pentobarbital sodium). The rats were prevented from feeling any pain by controlling their reflexes at intervals throughout the procedure and by administering an additional dose of anesthesia when necessary. After shaving, the incision areas were washed with povidone-iodine and all surgical procedures were performed under sterile conditions. After the surgical preparation of the lower extremities, ankle posterior line incisions were made and the Achilles tendons and plantar tendons were exposed. 0.2 cm partial lacerations were performed at 0.5 cm proximal to the calcaneus insertion of the middle of Achilles tendons, by using a flat blade with a width of 0.2 cm. Tendons were repaired end-to-end with 6/0 round polypropylene monofilament sutures. After washing the wounded areas with saline, the incisions were closed by using 4/0 polypropylene monofilament sutures and the integrity of the skins was achieved.

## In vivo trials of glucocorticoid treatment

The in vivo trials of glucocorticoid treatment were divided into two parts. First, we explored the response of representative animal models of the different tendinopathy subtypes to glucocorticoid treatment. Secondly, to more closely mimic clinical scenarios, we introduced lesion repair into the representative animal models and re-evaluated the efficacy of glucocorticoid treatment on the animal models. The subsequent paragraph describes the consistent experimental process for two parts of an in vivo trial.

20 rats (40 tendon samples) were allocated to the levofloxacin and collagenase models. After modeling for 2 weeks, half of the rats in each tendinopathy model were assigned to the glucocorticoid group and injected with 30 µL of compound betamethasone (J20140160) peri-tendinously, while the other half were assigned to the saline group. Explanted tendon samples were subjected to transcriptomic sequencing, histological evaluation, and transmission electron microscopy following euthanasia with excess pentobarbital sodium at 2 weeks post-treatment.

In the scenario of laceration repair, the levofloxacin and collagenase models underwent laceration repair modeling the day before hormone treatment, as described in section.

## Transcriptomic cross-species subtype analyses

Bioinformatics analyses were performed on human-rat orthologous genes. Gene expression was transformed and normalized using g:Profiler<sup>50</sup>. To categorize animal samples into human tendinopathy subtypes, opposing differentially-expressed genes were defined as the representative expression pattern of the subtypes ((Intersection genes of (Ir vs. normal control, FC > 2 and  $p < 0.05$ ) and (normal control vs. Hw, FC > 2 and  $p < 0.05$ ); intersection genes of (Ir vs. normal control, FC < -2 and  $p < 0.05$ ) and (normal control vs. Hw, FC < -2 and  $p < 0.05$ )). The nearest template prediction (NTP) module<sup>51</sup> in GenePattern<sup>52</sup> was used to find the nearest template to assign a prediction subtype to an animal sample.

Integrative pathway enrichment analysis across species was conducted using the ActivePathways R package (v2.0.0)<sup>53</sup>. ActivePathways combines transcriptomic datasets from different subtypes of tendinopathy patients and various animal models. Specifically, the input data consists of lists of differentially expressed genes (tendinopathy-specific subtypes versus normal human controls; specific animal models versus normal animal controls). ActivePathways prioritizes genes based on the significance ( $p$ -values from differential gene analysis) and direction (Log<sub>2</sub>FC from differential gene analysis) of signals



from datasets, and performs pathway enrichment analysis of these prioritized genes.

### Identification of the most influential transcriptional regulators

Differentially expressed genes were used for over-representation analysis to acquire key transcriptional regulators in GeneTrail. The top 50 TFs in each circumstance were selected according to the adjusted  $p$ -value.

### Protein-protein interaction (PPI) network construction and visualization

Using the STRING database (v.12.0), we constructed the PPI network with a medium confidence score of 0.4 using differentially expressed genes as input. The tab-separated values format file was downloaded and imported into Cytoscape (v.3.9.1) for subsequent interaction calculation. According to node degree, 12 key proteins were selected to construct a visual network.

### Analysis of microscopic structure by TEM

Tissue samples ( $n = 3$ ) were prepared using standard procedures for TEM<sup>46</sup>. Briefly, samples were pre-fixed with 2% (w/v) glutaraldehyde for 2 h at 4 °C and then washed twice with PBS at 4 °C followed by post-fixation with 1% (w/v) osmic acid for 2 h at 4 °C. After two washes in PBS, the samples were dehydrated with increasing ethanol gradient solutions and dried to a critical point. The samples were subsequently mounted and sputter-coated with gold for viewing under TEM (Quanta 10 FEI). We sampled the same viewing area (at least 500 collagen fibrils) in each group to measure the distribution of collagen fibril diameters. The fibril diameter was calculated as the smallest diameter from the shortest axis of each fibril.

### Exercise protocol and measurement

The creation of the forced running model and the assessment of motor function were performed on a treadmill (SANS, SA101). Before the forced running protocol began, rats underwent a week of short running activity training (15 m/min, 30 min/day, 6 days/week, 0°). Following the training period, rats were subjected to treadmill activity under modified conditions (20 m/min, 6 days/week, 0°) for 1 h/day. A treadmill equipped with an electric shock grid was used to stimulate animals, and animals were continuously monitored and motivated by pushing them with the end of stainless-steel forceps whenever they refused to run. Through these efforts, most animals maintained their running states during the exercise period. Animals that persisted in their refusal to run were removed from the treadmill and reintroduced at a later time to complete the designated running time. A few rats completely refused to run even after several repeated trials, and these rats were excluded from the exercise procedure. In motor function evaluation, rats that had no prior acclimatization ran on the treadmill at an initial speed of 2 m/min followed by an incremental speed of 2 m/min<sup>2</sup> until they reached a predefined exhaustion (>700 shocks at 1 mA of stimulation).

### Clinical data of glucocorticoid therapy

Patients received a local injection of 2 mL Compound Betamethasone Injection based on routine surgical sutures during surgery. Follow-ups were conducted at 6 and 24 months postoperatively. ROM of the shoulder joint, and OSS were collected. Differences in the improvement of these indicators were compared among the three subtypes.

### Statistical analysis

Statistical analysis was performed using R software (version 4.2.0, The R Project for Statistical Computing, [www.r-project.org](http://www.r-project.org)). Normality was assessed by the Shapiro-Wilk normality test. Levene's test was performed for the examination of equal variance. When variables presented normal distribution and equal variance, the student's  $t$ -test was

performed for the comparison of data between two groups, and one-way analysis of variance (ANOVA) was used for multiple group comparisons. Data failing normality or equal variance were analyzed by the Mann-Whitney  $U$  test or Kruskal-Wallis test. Categorical or dichotomous variables were compared using the chi-squared test or Fisher's exact test. All statistical tests are two-sided. The significance level is presented as \* $p < 0.05$ , \*\* $p < 0.01$ , \*\*\* $p < 0.001$  or \*\*\*\* $p < 0.0001$ . Values of  $p < 0.05$  were considered to be statistically significant. Analyses of transcriptional data were conducted in the R software.

### Reporting summary

Further information on research design is available in the Nature Portfolio Reporting Summary linked to this article.

### Data availability

The data that support the findings of this study—including clinical information, and transcriptome data—are available within the paper. The raw sequence data reported in this paper have been deposited in the Genome Sequence Archive in National Genomics Data Center, China National Center for Bioinformation / Beijing Institute of Genomics, Chinese Academy of Sciences (GSA: [HRA006534](https://ngdc.cncb.ac.cn/gsa/HRA006534), GSA: [CRA014406](https://ngdc.cncb.ac.cn/gsa/CRA014406)) that are publicly accessible at <https://ngdc.cncb.ac.cn/gsa><sup>54,55</sup>. Source data are provided with this paper.

### Code availability

Data analyses were carried out using either an assortment of R system software (<http://www.r-project.org>, 4.2.0) packages including those of Bioconductor or original R code. This paper does not report original code.

### References

1. Millar, N. L. et al. Tendinopathy. *Nat. Rev. Dis. Primers* **7** (2021).
2. Littlewood, C., Ashton, J., Chance-Larsen, K., May, S. & Sturrock, B. Exercise for rotator cuff tendinopathy: a systematic review. *Physiotherapy* **98**, 101–109 (2012).
3. Kim, J., Ryu, Y. & Kim, S. H. Surgical options for failed rotator cuff repair, except arthroplasty: review of current methods. *Clin. Shoulder Elb.* **23**, 48–58 (2020).
4. Cook, T., Minns Lowe, C., Maybury, M. & Lewis, J. S. Are corticosteroid injections more beneficial than anaesthetic injections alone in the management of rotator cuff-related shoulder pain? A systematic review. *Br. J. Sports Med.* **52**, 497–504 (2018).
5. Hopewell, S. et al. GRASP Trial Group, progressive exercise compared with best practice advice, with or without corticosteroid injection, for the treatment of patients with rotator cuff disorders (GRASP): a multicentre, pragmatic, 2 × 2 factorial, randomised controlled trial. *Lancet* **398**, 416–428 (2021).
6. Puzzitiello, R. N. et al. Adverse impact of corticosteroids on rotator cuff tendon health and repair: a systematic review of basic science studies. *Arthrosc. Sports Med. Rehabil.* **2**, e161–e169 (2020).
7. Mohamadi, A., Chan, J. J., Claessen, F. M., Ring, D. & Chen, N. C. Corticosteroid injections give small and transient pain relief in rotator cuff tendinosis: a meta-analysis. *Clin. Orthop. Relat. Res.* **475**, 232–243 (2017).
8. Lin, M. T. et al. Comparative effectiveness of injection therapies in rotator cuff tendinopathy: a systematic review, pairwise and network meta-analysis of randomized controlled trials. *Arch. Phys. Med. Rehabil.* **100**, 336–349.e15 (2019).
9. Kim, Y. S. et al. Is it safe to inject corticosteroids into the glenohumeral joint after arthroscopic rotator cuff repair. *Am. J. Sports Med.* **47**, 1694–1700 (2019).
10. Lädermann, A. et al. Classification of full-thickness rotator cuff lesions: a review. *EFORT Open Rev.* **1**, 420–430 (2016).
11. King, D. et al. Quadriceps tendinopathy: a review, part 2-classification, prognosis, and treatment. *Ann. Transl. Med.* **7**, 72 (2019).

12. Guinney, J. et al. The consensus molecular subtypes of colorectal cancer. *Nat. Med.* **21**, 1350–1356 (2015).
13. Seiler, R. et al. Divergent biological response to neoadjuvant chemotherapy in muscle-invasive bladder cancer. *Clin. Cancer Res.* **25**, 5082–5093 (2019).
14. Neff, R. A. et al. Molecular subtyping of Alzheimer's disease using RNA sequencing data reveals novel mechanisms and targets. *Sci. Adv.* **7** (2021).
15. Soul, J. et al. Stratification of knee osteoarthritis: two major patient subgroups identified by genome-wide expression analysis of articular cartilage. *Ann. Rheum. Dis.* **77**, 423 (2018).
16. Orange, D. E. et al. Accelerating medicines partnership in rheumatoid arthritis and lupus network, V. P. Bykerk, S. M. Goodman, L. T. Donlin, identification of three rheumatoid arthritis disease subtypes by machine learning integration of synovial histologic features and RNA sequencing data. *Arthritis Rheumatol.* **70**, 690–701 (2018).
17. Luo, J. et al. Animal model for tendinopathy. *J. Orthop. Transl.* **42**, 43–56 (2023).
18. Bedi, A. et al. Rotator cuff tears. *Nat. Rev. Dis. Prim.* **10**, 8 (2024).
19. Zheng, K., Yu, S., Chen, L., Dang, L. & Chen, B. BPI-GNN: Interpretable brain network-based psychiatric diagnosis and subtyping. *Neuroimage* **292**, 120594 (2024).
20. Fan, H. et al. Artificial intelligence-based MRI radiomics and radiogenomics in glioma. *Cancer Imaging* **24**, 36 (2024).
21. Pan, L. et al. The prevalence, awareness, treatment and control of dyslipidemia among adults in China. *Atherosclerosis* **248**, 2–9 (2016).
22. Fang, W. H., Bonavida, V., Agrawal, D. K. & Thankam, F. G. Hyperlipidemia in tendon injury: chronicles of low-density lipoproteins. *Cell Tissue Res.* **392**, 431–442 (2023).
23. Alves, C., Mendes, D. & Marques, F. B. Fluoroquinolones and the risk of tendon injury: a systematic review and meta-analysis. *Eur. J. Clin. Pharmacol.* **75**, 1431–1443 (2019).
24. Hussain, T. et al. Oxidative stress and inflammation: what polyphenols can do for us. *Oxid. Med. Cell Longev.* **2016**, 7432797 (2016).
25. Furuta, H. et al. Increased expression of glutathione peroxidase 3 prevents tendinopathy by suppressing oxidative stress. *Front. Pharm.* **14**, 1137952 (2023).
26. Duran, E., Bilgin, E., Ertenli, A. İ. & Kalyoncu, U. The frequency of Achilles and plantar calcaneal spurs in gout patients. *Turk. J. Med. Sci.* **51**, 1841–1848 (2021).
27. Jiang, G. et al. Comparison of leukocyte-rich platelet-rich plasma and leukocyte-poor platelet-rich plasma on achilles tendinopathy at an early stage in a rabbit model. *Am. J. Sports Med.* **48**, 1189–1199 (2020).
28. Kokubu, S., Inaki, R., Hoshi, K. & Hikita, A. Adipose-derived stem cells improve tendon repair and prevent ectopic ossification in tendinopathy by inhibiting inflammation and inducing neovascularization in the early stage of tendon healing. *Regen. Ther.* **14**, 103–110 (2020).
29. Burton, I. Combined extracorporeal shockwave therapy and exercise for the treatment of tendinopathy: a narrative review. *Sports Med. Health Sci.* **4**, 8–17 (2022).
30. Smallcomb, M., Khandare, S., Vidt, M. E. & Simon, J. C. Therapeutic ultrasound and shockwave therapy for tendinopathy: a narrative review. *Am. J. Phys. Med. Rehabil.* **101**, 801–807 (2022).
31. Aljefri, A. M. et al. Clinical applications of PRP: musculoskeletal applications, current practices and update. *Cardiovasc. Interv. Radio.* **46**, 1504–1516 (2023).
32. Docheva, D., Müller, S. A., Majewski, M. & Evans, C. H. Biologics for tendon repair. *Adv. Drug Deliv. Rev.* **84**, 222–239 (2015).
33. Da, H., Song, J. K., Liu, L. & Zhou, L. Compound betamethasone in the treatment of pain after supraspinatus tendon repair. *J. Int. Med. Res.* **50**, 3000605221121962 (2022).
34. Moosmayer, S. et al. Ultrasound guided lavage with corticosteroid injection versus sham lavage with and without corticosteroid injection for calcific tendinopathy of shoulder: randomised double blinded multi-arm study. *BMJ* **383**, e076447 (2023).
35. Coombes, B. K., Bisset, L., Brooks, P., Khan, A. & Vicenzino, B. Effect of corticosteroid injection, physiotherapy, or both on clinical outcomes in patients with unilateral lateral epicondylalgia: a randomized controlled trial. *JAMA* **309**, 461–469 (2013).
36. Harada, Y. et al. Dose- and time-dependent effects of triamcinolone acetonide on human rotator cuff-derived cells. *Bone Jt. Res.* **3**, 328–334 (2014).
37. Kafa, B. et al. Histological and biomechanical effects of local anesthetics and steroids on achilles tendon: a study in rats. *Am. J. Sports Med.* **51**, 1319–1327 (2023).
38. Trapnell, C., Pachter, L. & Salzberg, S. L. TopHat: discovering splice junctions with RNA-Seq. *Bioinformatics* **25**, 1105–1111 (2009).
39. Pascual-Montano, A., Carazo, J. M., Kochi, K., Lehmann, D. & Pascual-Marqui, R. D. Nonsmooth nonnegative matrix factorization (nsNMF). *IEEE Trans. Pattern Anal. Mach. Intell.* **28**, 403–415 (2006).
40. Brunet, J. P., Tamayo, P., Golub, T. R. & Mesirov, J. P. Metagenes and molecular pattern discovery using matrix factorization. *Proc. Natl Acad. Sci. USA* **101**, 4164–4169 (2004).
41. Love, M. I., Huber, W. & Anders, S. Moderated estimation of fold change and dispersion for RNA-seq data with DESeq2. *Genome Biol.* **15**, 550 (2014).
42. Hänzelmann, S., Castelo, R. & Guinney, J. GSEA: gene set variation analysis for microarray and RNA-seq data. *BMC Bioinform.* **14**, 7 (2013).
43. Aran, D., Hu, Z. & Butte, A. J. xCell: digitally portraying the tissue cellular heterogeneity landscape. *Genome Biol.* **18**, 220 (2017).
44. Song, W. M. & Zhang, B. Multiscale embedded gene co-expression network analysis. *PLoS Comput. Biol.* **11**, e1004574 (2015).
45. Zhang, B. & Zhu, J. Identification of key causal regulators in gene networks. *Proc. World Congr. Eng.* **2**, 5–8 (2013).
46. Ruan, D. et al. Early-stage primary anti-inflammatory therapy enhances the regenerative efficacy of platelet-rich plasma in a rabbit achilles tendinopathy model. *Am. J. Sports Med.* **49**, 3357–3371 (2021).
47. Zhao, B. A. et al. Role of the Alarmin S100A9 protein in inducing Achilles tendinopathy in rats. *Ann. Transl. Med.* **9**, 1698 (2021).
48. Feuerriegel, G. C. et al. Fat fractions of the rotator cuff muscles acquired with 2-point Dixon MRI: predicting outcome after arthroscopic rotator cuff repair. *Invest. Radiol.* **59**, 328–336 (2023).
49. Ishitani, E. et al. Tendon stump type on magnetic resonance imaging is a predictive factor for retear after arthroscopic rotator cuff repair. *J. Shoulder Elb. Surg.* **28**, 1647–1653 (2019).
50. Raudvere, U. et al. g:Profiler: a web server for functional enrichment analysis and conversions of gene lists (2019 update). *Nucleic Acids Res.* **47**, W191–W191W198 (2019).
51. Hoshida, Y. Nearest template prediction: a single-sample-based flexible class prediction with confidence assessment. *PLoS ONE* **5**, e15543 (2010).
52. Reich, M. et al. GenePattern 2.0. *Nat. Genet.* **38**, 500–501 (2006).
53. Paczkowska, M. et al. Integrative pathway enrichment analysis of multivariate omics data. *Nat. Commun.* **11**, 735 (2020).
54. Chen, T. et al. The genome sequence archive family: toward explosive data growth and diverse data types. *Genomics Proteom. Bioinform.* **19**, 578–583 (2021).
55. CNCR-NGDC Members and Partners. Database Resources of the National Genomics Data Center, China National Center for Bioinformatics in 2024. *Nucleic Acids Res.* **52**, D18–D18D32 (2024).

## Acknowledgements

The work of our research group was supported by NSFC grants (T2121004 to H.O. and X.C., 82372376 to W.S., 82301766 to C.T.), Zhejiang Lingyan project(2024C03207 to W.S.), Medical Health Science and Technology Project of Zhejiang Provincial Health Commission (Grant No. 2022RC161 to W.S.), Zhejiang Provincial Program for the Cultivation of High-level Innovative Health Talents (W.S.), Dr. Li Dak Sum & Yip Yio Chin Regeneration Medicine Foundation (W.S.), China Postdoctoral Science Foundation (2022M712762 to C.T.), Postdoctoral Program of Binjiang Institute of Zhejiang University (ZX202111SMKY001 to C.T.) and Key R&D Program of Zhejiang (2024C03077 to W.S.). We thank Kefeng Ding, Weiting Ge and Tongtong Bu from SAHZU Biobank and SAHZU Center of Basic and Translational Research for their technical support (SAHZU: The Second Affiliated Hospital, Zhejiang University School of Medicine). Figure 3H was constructed from the image initially created with Bionder (<https://www.biorender.com/>) and subsequently modified. Figure 4A was drawn in part using images from Servier Medical Art. Servier Medical Art by Servier is licensed under a Creative Commons Attribution 3.0 Unported License (<https://creativecommons.org/licenses/by/3.0/>).

## Author contributions

C.T., W.S., X.C., H.O., W.C., Z.Y., J.L., and H.W. conceived the study; C.T., Z.W., and Y.X. designed experiments, performed the analyses, prepared the figures and wrote the paper. Y.F., C.W., P.H., and H.L. collected clinical samples and medical history information. J.L. and R.Y. performed bioinformatics analysis. Y.C. and J.H. performed molecular experiment. Z.W. assisted in animal experiments. Y.Y. and Y.Z. optimized the figures. B.H. corrected grammatical errors.

## Competing interests

The authors declare no competing interest

## Additional information

**Supplementary information** The online version contains supplementary material available at <https://doi.org/10.1038/s41467-024-53826-w>.

**Correspondence** and requests for materials should be addressed to Hongwei Ouyang, Xiao Chen or Weiliang Shen.

**Peer review information** *Nature Communications* thanks Brian Feeley, Stavros Thomopoulos, and the other, anonymous, reviewer(s) for their contribution to the peer review of this work. A peer review file is available.

**Reprints and permissions information** is available at <http://www.nature.com/reprints>

**Publisher's note** Springer Nature remains neutral with regard to jurisdictional claims in published maps and institutional affiliations.

**Open Access** This article is licensed under a Creative Commons Attribution-NonCommercial-NoDerivatives 4.0 International License, which permits any non-commercial use, sharing, distribution and reproduction in any medium or format, as long as you give appropriate credit to the original author(s) and the source, provide a link to the Creative Commons licence, and indicate if you modified the licensed material. You do not have permission under this licence to share adapted material derived from this article or parts of it. The images or other third party material in this article are included in the article's Creative Commons licence, unless indicated otherwise in a credit line to the material. If material is not included in the article's Creative Commons licence and your intended use is not permitted by statutory regulation or exceeds the permitted use, you will need to obtain permission directly from the copyright holder. To view a copy of this licence, visit <http://creativecommons.org/licenses/by-nc-nd/4.0/>.

© The Author(s) 2024, corrected publication 2025

<sup>1</sup>Department of Sports Medicine & Orthopedic Surgery, the Second Affiliated Hospital, Zhejiang University School of Medicine, Hangzhou City, Zhejiang Province, China. <sup>2</sup>Institute of Sports Medicine, Zhejiang University, Hangzhou City, Zhejiang Province, China. <sup>3</sup>Key Laboratory of Motor System Disease Research and Precision Therapy of Zhejiang Province, Hangzhou City, Zhejiang Province, China. <sup>4</sup>Clinical Research Center of Motor System Disease of Zhejiang Province, Hangzhou City, Zhejiang Province, China. <sup>5</sup>Binjiang Institute of Zhejiang University, Hangzhou City, Zhejiang Province, China. <sup>6</sup>Dr. Li Dak Sum and Yip Yio Chin Center for Stem Cell and Regenerative Medicine, Zhejiang University, Hangzhou City, Zhejiang Province, China. <sup>7</sup>Orthopedics Research Institute of Zhejiang University, 310058 Hangzhou City, Zhejiang Province, China. <sup>8</sup>Department of Orthopedics, Huzhou Central Hospital, Affiliated Huzhou Hospital, Zhejiang University School of Medicine, Huzhou City, Zhejiang Province, China. <sup>9</sup>Key Laboratory of Reproductive Genetics (Ministry of Education) and Department of Reproductive Endocrinology, Women's Hospital, Zhejiang University School of Medicine, Hangzhou City, Zhejiang Province, China. <sup>10</sup>Department of Dental Materials & Dental Medical Devices Testing Center, Peking University School and Hospital of Stomatology, Beijing City, China. <sup>11</sup>China Orthopedic Regenerative Medicine Group (CORMed), Hangzhou City, Zhejiang Province, China. <sup>12</sup>Liangzhu Laboratory, Zhejiang University, Hangzhou City, Zhejiang Province, China. <sup>13</sup>State Key Laboratory of Transvascular Implantation Devices, Hangzhou City, Zhejiang Province, China. <sup>14</sup>These authors contributed equally: Chenqi Tang, Zetao Wang, Yuanhao Xie. ✉ e-mail: [hwoy@zju.edu.cn](mailto:hwoy@zju.edu.cn); [chenxiao-610@zju.edu.cn](mailto:chenxiao-610@zju.edu.cn); [wlishen@zju.edu.cn](mailto:wlishen@zju.edu.cn)